Available online at www.sciencedirect.com
ScienceDirect
Trans. Nonferrous Met. Soc. China 33(2023) 3185−3197
Transactions of Nonferrous Metals Society of China
www.tnmsc.cn

Purification of crude indium by two-stage cyclone electrowinning

Qing-hua TIAN[1,2], Bo DONG[1], Xue-yi GUO[1,2], Dong LI[1,2], Zou-jiang LI[1], Zhi-peng XU[1,2]

1. School of Metallurgy and Environment, Central South University, Changsha 410083, China;
2. National & Regional Joint Engineering Research Center of Nonferrous Metal Resource Recycling, Central South University, Changsha 410083, China

Received 5 May 2022; accepted 6 October 2022

Abstract: A possible process for the purification of crude indium by two-stage cyclone electrowinning was proposed. In accordance with a linear sweep voltammetry (LSV) results and the evaluation of the diffusion coefficient (D=6.15×10^{-11} cm^2/s), indium electrodeposition in $In_2(SO_4)_3$ solution was controlled by a diffusion-controlled irreversible process, and mass transfer can be significantly enhanced by electrolyte flow. During the 1st-stage indium cyclone electrowinning, a current efficiency (CE) of 80.15%, specific energy consumption (SEC) of 2.11 kW·h/kg and average cell voltage (ACV) of 2.04 V were achieved under the optimum conditions. Meanwhile, the purity of indium increased from 94.34% to 99.95%. During the 2nd-stage indium cyclone electrowinning, 98.95% purity of cathode indium was conducted by electrowinning under the optimum conditions, while the CE, SEC, and ACV were 75.23%, 2.23 kW·h/kg and 2.40 V, respectively. After two-stage cyclone electrowinning, the comprehensive recovery of indium is as high as 98.22%.

Key words: indium; cyclone electrowinning; electrochemical behavior; purification

1 Introduction

Indium is an important scattered metal. Due to its excellent optoelectronic properties, indium is widely used in high-precision fields such as electronic materials, semiconductors, and special alloy materials [1]. Indium-containing products, such as InP, InSe, InAs, copper indium selenide (CIS), copper indium gallium selenide (CIGS) and indium tin oxide (ITO), are essential for components of electronic and optoelectronic devices [2]. Therefore, the above products have increasingly stringent requirements for the purity of indium raw materials. Electrolysis is the most widely used method to prepare indium metal products. As a rule, electrolysis of indium is carried out in a conventional parallel electrolytic cell with crude indium as the anode and a titanium plate as the cathode [3]. The electrolyte is prepared by dissolving high purity indium (>99.99%) into sulfuric acid, and NaCl is added as a conductive agent [4]. KANG et al [5] obtained high purity indium (>99.99%) by electrolytic refining of indium from chloride solution in a conventional parallel electrolytic cell, but >99.50% purity of the electrolyte was needed. LEE and OH [6] studied the electrowinning of indium from chloride solutions at a current density of 100 mA/cm^2. A current efficiency (CE) of 90% was achieved when both the initial concentrations of indium and NaCl were higher than 50 g/L. However, because of the presence of Cl^- in the electrolyte, Cl_2 was produced at the anode, which caused environmental risk. The indium electrolysis process is available worldwide because of its applicability. However, it has some important limitations [7−9]: (1) The Sn, Cd and Tl impurity levels in the crude indium anode and

Corresponding author: Zhi-peng XU, Tel: +86-731-88876839, E-mail: zhipeng.xu@csu.edu.cn
DOI: 10.1016/S1003-6326(23)66326-5

electrolyte should be strictly controlled; (2) Many waste anodes are produced during the electrolysis process, accounting for more than 40% of indium anodes; (3) The indium concentration needs to be kept at 70−80 g/L during the electrolysis process, resulting in a large backlog of funds. Consequently, it is of great interest to develop an efficient method for indium electrolysis.

Cyclone electrowinning is an efficient, selective, and readily adaptable method to recover metal/metalloid ions from an aqueous solution [10,11]. By introducing a high flow rate of electrolytes, the diffusion layer thickness decreases considerably in the cyclone electrowinning process [12,13]. The mass transfer is effectively enhanced by the turbulence developed by the high flow rate of the electrolyte [14]. Moreover, the concentration polarization, which tends to slow down the rate of anodic and cathodic reactions, is greatly reduced [15]. It has been reported that this technology has been used in the electrowinning of metals with good results, such as Cu, Sn, Bi, Sb, Te, Se, and Pt [16−18]. GUO et al [16] recovered copper from sulfuric acid leaching solution by cyclone electrowinning at a high current density of 400 A/m^2, while 99.98% purity of cathode copper and 94.96% CE were obtained. Tellurium was efficiently electrodeposited from an alkaline solution by cyclone electrowinning with a CE of 95.25% [17]. However, the purification of crude indium by cyclone electrowinning is seldom reported in the literature. The existing drawbacks of indium conventional parallel electrolytic refining may be overcome by cyclone electrowinning technology, and the indium electrodeposition process may be enhanced at the same time. That is, cyclone electrowinning may serve as a promising alternative for efficient electrodeposition of indium from an aqueous solution.

In the present study, a possible purification process for crude indium by two-stage cyclone electrowinning was proposed. The electrochemical behavior of indium(III) in sulfate media was studied by linear sweep voltammetry (LSV). The effects of various parameters, including current density, electrolyte flow rate, electrolyte temperature, and electrolysis time on various indexes of two-stage indium cyclone electrowinning were systematically investigated.

2 Experimental

2.1 Materials

The crude indium used in the experiments was provided by First Rare Materials Co., Ltd., Guangdong Province, China. The chemical composition of crude indium is listed in Table 1. This result indicated that in addition to In (94.34%), the following main elements were found: Bi 1.95%, Pb 1.48%, Sn 0.99%, and Si 0.75%. The chemical reagents used in this study were all of analytical grade.

Table 1 Chemical composition of crude indium (wt.%)

In	Bi	Pb	Sn	Si	Cd	Cu	Others
94.34	1.95	1.48	0.99	0.75	0.40	0.04	0.05

2.2 Equipment and procedures

A standard three-electrode cell was employed in all electrochemical experiments. The working electrode was a 316 L stainless steel plate (1 cm × 1 cm), the counter electrode was a Pt plate (1.5 cm × 1.5 cm), and the reference electrode was a saturated calomel electrode (0.24 V vs SHE, 25 °C). All electrochemical measurements were carried out at 25 °C using an electrochemical workstation (PGSTAT302N, Metrohm, Switzerland).

Figure 1 shows the schematic diagram of two-stage cyclone electrowinning. The cyclone electrowinning cell had an IrO_2−Ta_2O_5-coated titanium anode in the center, with 316 L annular stainless steel foil cathode surrounding the anode. The area of the cathode was 400 cm^2, and the distance between the cathode and anode was 3 cm. The electrolytes used in the indium cyclone electrowinning experiments were prepared by dissolving crude indium in concentrated sulfuric acid (98 wt.%). Then, sodium hydroxide was used to adjust the pH of the electrolytes to a value of 2. Table 2 lists the chemical composition of the prepared indium electrolyte. The 2 L of the prepared indium electrolyte was used in each electrowinning experiment. A high-precision DC power supply (RXN−1520D, Zhaoxin, China) was applied to maintaining a constant current. During the electrowinning process, sodium hydroxide solution (3 mol/L) was pumped to the electrolyte by a peristaltic pump at a constant speed to keep the

pH of the electrolyte at 2. The amount of sodium hydroxide pumped into the electrolyte was depended on the applied current and electrolysis time. After electrowinning, the indium deposits obtained at the cathode were washed with deionized water three times and dried in an oven at approximately 50 °C for 12 h.

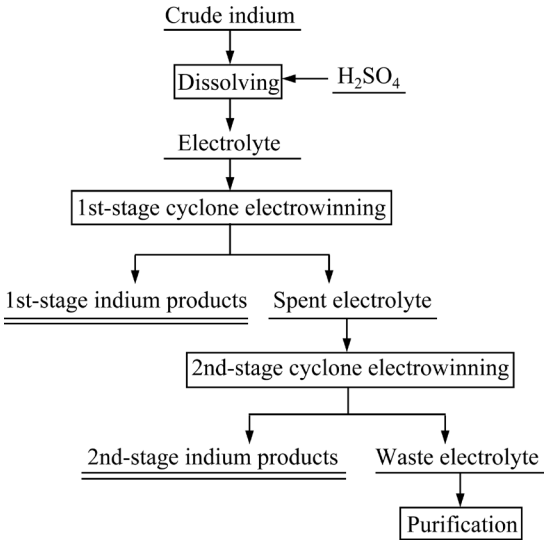

Fig. 1 Proposed flowsheet for purification of crude indium by two-stage cyclone electrowinning

Table 2 Chemical composition of electrolyte (g/L)

In	Bi	Pb	Sn	Si	Cd	Cu	Ni	Fe
68.20	1.41	1.08	0.72	0.54	0.50	0.05	0.02	0.01

The calculation formula for the current efficiency (η) of the electrowinning process is shown in Eq. (1):

$$\eta=\omega m/(qIt) \quad (1)$$

where m (g) is the actual mass of indium deposits, ω is the purity of indium deposits, q is the electrochemical equivalent mass of indium (1.428 $g\cdot A^{-1}\cdot h^{-1}$), I (A) is the applied current and t (h) is the electrolysis time.

The recovery of indium (r, %) for the electrowinning process is calculated using Eq. (2):

$$r=(C_1V_1-C_2V_2)/C_1V_1\times100\% \quad (2)$$

where C_1 (g/L) is the initial concentration of indium in the electrolyte, V_1 (L) is the initial volume of electrolyte, C_2 (g/L) is the final concentration of indium in the electrolyte after electrowinning and V_2 (L) is the final volume of electrolyte.

The specific energy consumption (SEC) (W, $kW\cdot h\cdot kg^{-1}$) is calculated according to Eq. (3):

$$W=E/(q\eta) \quad (3)$$

where E (V) is the average cell voltage (ACV).

The volume of sodium hydroxide solution pumped into electrolyte (V_3, L) can be calculated using Eq. (4):

$$V_3=3600It/(FC_3) \quad (4)$$

where F is Faraday's constant, and C_3 is the concentration of the sodium hydroxide solution (3 mol/L).

2.3 Characterization methods

The chemical compositions of the crude indium, indium deposits and electrolytes were determined by inductively coupled plasma atomic emission spectrometry (ICP) (Optima 5300DV, Perkin Elmer, USA). XRD patterns of indium deposits were collected using a Bruker D8−Discover diffractometer in the 2θ range of 10°−80° at a scanning rate of 1 (°)/min with Cu K_α radiation. The cell voltage was measured using a digital universal meter (UT61E, UNI−T, China).

3 Results and discussion

3.1 Electrochemical behavior of indium(III) ions in sulfate media

The electrodeposition of indium from aqueous solutions has been extensively studied and is well understood [19]. The first reliable determination of the In^{3+}/In potential was reported by HAKOMORI [20]. The standard reduction potential of the In^{3+}/In couple is −0.34 V [21]. This was followed by the investigations of HATTOX and VRIES [22], KANGRO and WEINGÄRTNER [23], LIETZKE and STOUGHTON [24], COVINGTON et al [25] and HAMPSON and PIERCY [26]. For the study of the electrodeposition of indium, one of the important variables is the electrolyte used [21]. Most studies of the electrodeposition of indium have been carried out in perchlorate, chloride, cyanide, tartrate, formate, sulfate and halide sulfate [6,21]. Sulfate electrolytes have been the most extensively studied and the most widely used commercially by virtue of their relative simplicity [27]. Most studies have been focused on using In^{3+}+H_2SO_4 as an electrolyte, by adding NaCl as a supporting electrolyte, and gelatin as an additive [28]. The electrolyzer was separated by a cation membrane, and electrolytic refining was carried out with crude indium as the anode and a

titanium plate as the cathode [29]. However, the electrochemical behaviors of indium are different under different electrolyte systems [30]. The electrochemical behavior of indium in $In_2(SO_4)_3$ solution has not been reported in the literature. A few research groups reported the systematic study of electrochemical kinetics during the electrodeposition of indium [31]. In accordance with the voltamperometric study and the evaluation of the diffusion coefficient, D, indium electrodeposition was controlled by a diffusion process at a high current density [21]. The mass transfer of the liquid phase can be enhanced, and the concentration polarization can be reduced by strengthening stirring and increasing the temperature [32]. However, the control steps and related kinetic parameters of the electrodeposition process in $In_2(SO_4)_3$ solution are not clear.

The electrochemical behavior of indium in $In_2(SO_4)_3$ solution was studied by the LSV measurements at 25 °C. Figure 2 shows the LSV curve of $In_2(SO_4)_3$ solution (65 g/L In^{3+}, pH=2) and H_2SO_4 (blank) solution (pH=2). It can be seen from the LSV curve of the blank solution that the current density started to increase when the potential shifted to approximately −0.40 V. The current density increased with the potential shifting negatively, indicating that hydrogen evolution occurred at the cathode [21]. In addition, a clear reduction peak (marked as Peak C_1) at −0.75 V with a peak current density of 6.20 mA/cm^2 was observed in the presence of In^{3+}, while there was no reduction peak in the forward scan of the blank solution. This suggested that Peak C_1 was attributed to the reduction of indium(III) ions to indium(0) [33,34].

To identify the controlling step of the indium electrodeposition process, LSV measurements of the $In_2(SO_4)_3$ solution (65 g/L In^{3+}, pH=2) were performed at different potential scan rates ranging from 2 to 20 mV/s at 25 °C (Fig. 3). As the scan rate increased, a negative shift of the C_1 cathodic peak potential and an increase in the peak current were observed. This suggests that the indium electrodeposition process is a diffusion-controlled irreversible reaction [6]. For a diffusion-controlled reaction, there is

$$I_p = 0.4463\frac{(nF)^{3/2}}{(RT)^{1/2}}AD^{1/2}Cv^{1/2} \quad (5)$$

where I_p (A) is the peak current, n is the number of electrons, R (8.314 J/(mol·K)) is the molar gas constant, T (K) is the thermodynamic temperature, A (cm^2) is the surface area of the working electrode, D (cm^2/s) is the diffusion coefficient, C (mol/mL) is the bulk concentration, and v (V/s) is the scan rate.

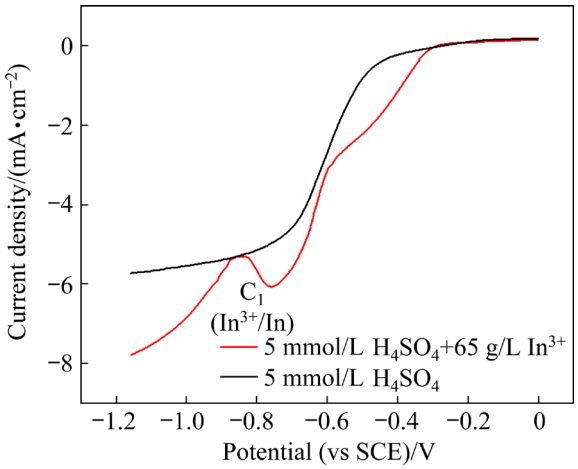

Fig. 2 LSV curves of $In_2(SO_4)_3$ solution and blank solution (Scan rate: 5 mV/s)

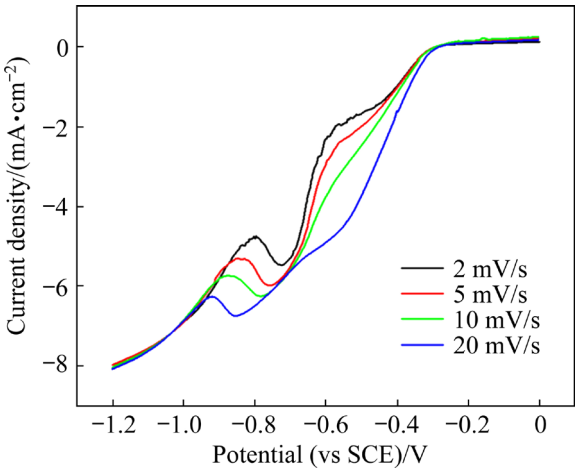

Fig. 3 LSV curves of $In_2(SO_4)_3$ solution at different scan rates

Figure 4 illustrates the relationship between the C_1 cathodic peak current and the square root of the scan rate ($v^{1/2}$). The plots exhibited a good linear relationship, suggesting that indium electrodeposition was diffusion-controlled [17]. According to Eq. (5), the diffusion coefficient of In^{3+} at 25 °C was estimated to be 6.15×10^{-11} cm^2/s. It can be found that the diffusion coefficient is relatively low, which may be expected to be overcome by cyclone electrowinning technology for better recovery and purification performance.

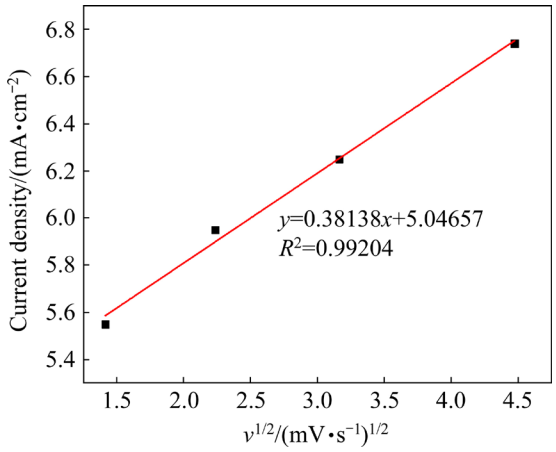

Fig. 4 Variation in reduction peak current as function of square root of scan rate

3.2 1st-stage indium cyclone electrowinning

3.2.1 Effect of current density

The influence of current density on the 1st-stage indium cyclone electrowinning was carried out at a flow rate of 200 L/h and electrolyte temperature of 30 °C for 20 h with a current density from 40 to 120 A/m^2. The effect of current density on CE and recovery of indium is shown in Fig. 5(a). It can be observed that the CE decreased from 83.31% to 63.40% with an increase in current density from 40 to 120 A/m^2. The above phenomenon is ascribed to the fact that the hydrogen evolution at the cathode was enhanced by increasing the current density [35]. The rate of the electrodeposition reaction was much higher than the diffusion rate at a higher current density, resulting in hydrogen evolution becoming a major reaction on the cathode. These results are similar to the electrodeposition of zinc in acid solutions, where hydrogen evolution becomes more intense at higher current densities [36]. Meanwhile, the recovery of indium increased from 28.20% to 66.77% with increasing current density. Figure 5(b) shows the effect of the current density on the ACV and SEC. With increasing the current density from 40 to 120 A/m^2, the ACV increased from 2.44 to 2.78 V. These results are consistent with the results reported by DELL'ERA et al [37] that as the current density increased, the cathodic and anodic overpotentials rose, leading to an increase in the cell voltage. On the other hand, SEC increased from 2.04 to 3.07 kW·h/kg with increasing current density.

During the electrodeposition of indium, in addition to the reduction of indium and the hydrogen evolution reaction in the cathode, some impurities in the electrolyte can also codeposit with indium, which affects product quality and technical indicators. The specific reaction equation and standard reduction potential are given in Table 3. Table 3 shows that the standard reduction potential of impurities nickel, tin, lead, and bismuth is more positive than that of indium, so it is easy to deposit on the cathode during the electrowinning process. In particular, the properties of tin, lead, and indium

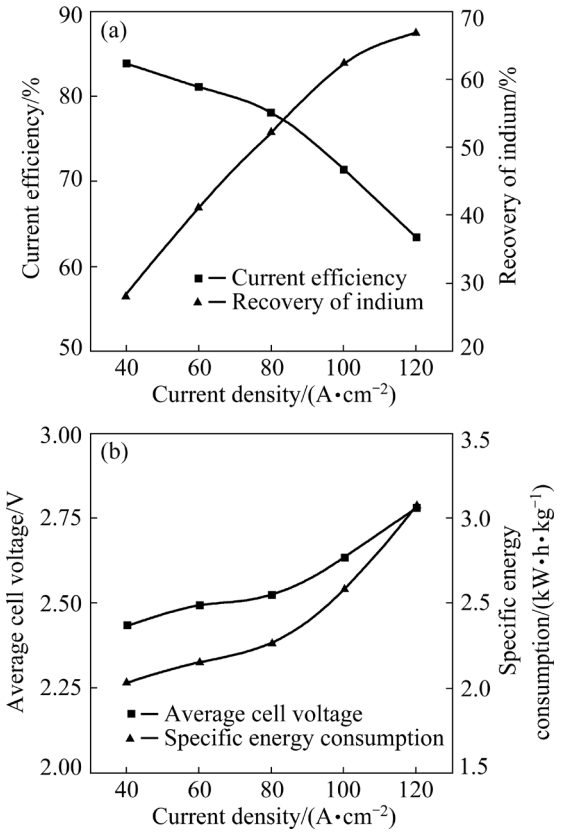

Fig. 5 Effect of current density on various indexes of 1st-stage indium cyclone electrowinning: (a) CE and recovery of indium; (b) ACV and SEC

Table 3 Typical reduction reaction and standard reduction potential in sulfate electrolyte

Reduction reaction	Standard reduction potential/V
$Fe^{2+} + 2e = Fe$	−0.440
$Cd^{2+} + 2e = Cd$	−0.403
$In^{3+} + 3e = In$	−0.343
$Ni^{2+} + 2e = Ni$	−0.257
$Sn^{2+} + 2e = Sn$	−0.136
$Pb^{2+} + 2e = Pb$	−0.126
$2H^{+} + 2e = H_2$	0
$Bi^{3+} + 3e = Bi$	0.308

are similar, and they are easy to codeposit with indium during electrowinning. Although the standard reduction potential of the impurities iron and cadmium is more negative than that of indium, it is very close to the reduction potential of indium, so it is also easy to codeposit with indium.

The main impurity content of the product at different current densities is given in Table 4. As shown in Table 4, the main impurities in the product are Sn, Cd, Pb, Bi, Ni, and Fe. When the current density is low, the contents of impurities Sn, Cd, Pb, Bi, etc., decrease with increasing current density. However, as the current density further increases, the electrodeposition of impurities is strengthened so that the impurity content in the product increases. After calculation, the purity of indium obtained by cyclone electrowinning at all current densities reaches more than 99.9%. Based on the above results, 80 A/m^2 was considered the optimum current density, which was higher than that applied in indium electrolysis (60 A/m^2).

Table 4 Main impurity content of cathode indium at different current densities (10^{-6})

Current density/ (A·m^{-2})	Sn	Cd	Pb	Bi	Ni	Fe
40	206.4	250.1	96.9	134.9	15.3	19.8
60	138.3	248.1	62.7	107.2	7.6	5.0
80	155.3	215.1	63.9	92.6	7.3	6.7
100	292.0	227.2	143.3	179.2	7.3	8.3
120	296.0	261.3	164.1	196.0	13.4	21.2

3.2.2 Effect of electrolyte flow rate

The effect of the electrolyte flow rate was determined by varying the flow rate of the electrolyte in the range from 100 to 500 L/h using current density of 80 A/m^2 at 30 °C for 20 h. As shown in Fig. 6(a), the CE increased by 4.63% from 100 to 300 L/h. This was attributed to the fact that the diffusion layer thickness of the electrolyte near the cathode decreased with increasing electrolyte flow rate. The CE showed a value of more than 80% at 300 L/h. However, the CE decreased sharply to approximately 30% at a flow rate of 500 L/h. This was because the indium deposits were washed away from the cathode by the high-speed electrolyte flow and came into contact with the anode rod, resulting in a short circuit in the electrolytic cell (Fig. 7). In addition, the movement of hydrogen ions was enhanced by the high flow rate electrolyte so that the charge transfer was beneficial to the hydrogen evolution. Figure 6(b) shows that ACV decreased from 2.55 to 2.51 V by increasing the electrolyte flow rate from 100 to 300 L/h. This is due to the enhanced mass transfer

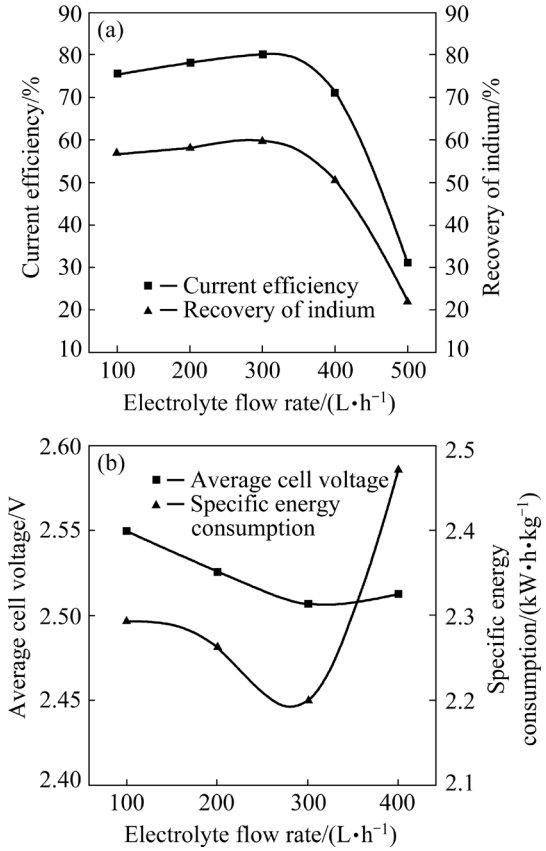

Fig. 6 Effect of electrolyte flow rate on various indexes of 1st-stage indium cyclone electrowinning: (a) CE and recovery of indium; (b) ACV and SEC

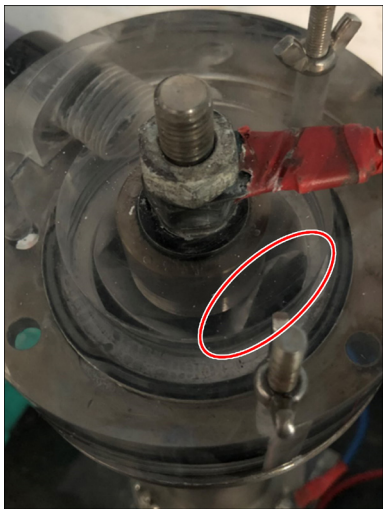

Fig. 7 Deposited indium in electrolytic cell at flow rate of 500 L/h

and decreased concentration polarization at a higher electrolyte flow rate [38]. When the flow rate increased to 400 L/h, the ACV performed a slight increase to 2.52 V. As mentioned above, at an electrolyte flow rate of 500 L/h, a short circuit occurred, which caused the cell voltage during the experiment to be unmeasurable. The energy consumption of a kilogram of indium was seen to decrease from 2.29 to 2.20 kW·h with increasing the electrolyte flow rate from 100 to 300 L/h and then increased sharply to 2.47 kW·h at 400 L/h.

The main impurity content of indium products at different electrolyte flow rates is given in Table 5. It can be seen that the electrolyte flow rates have little effect on the content of Ni and Fe in the product but have a greater effect on the content of Sn, Cd, Pb and Bi. The contents of Sn, Cd, Pb and Bi decreased with increasing electrolyte flow rate from 100 to 300 L/h, and the impurity content reached its lowest value at 300 L/h. Because the increase in the electrolyte flow rate reduces the thickness of the diffusion layer so that the indium ions in the electrolyte near the cathode can be quickly replenished, the deposition of indium is strengthened, and the precipitation of impurity ions is reduced. At a high electrolyte flow rate, the short-circuit phenomenon of the electrodeposition cell causes impurity ions to easily codeposit with indium. Therefore, the impurity content in the product increases sharply. In summary, an appropriate range of electrolyte flow rates is beneficial to indium deposition. A flow rate of 300 L/h was considered the optimum flow rate of electrolyte for subsequent experiments.

Table 5 Main impurity content of cathode indium at different electrolyte flow rates (10^{-6})

Flow rate/(L·h^{-1})	Sn	Cd	Pb	Bi	Ni	Fe
100	154.3	217.6	86.2	88.4	7.88	7.8
200	155.3	215.1	63.9	92.6	7.3	6.7
300	136.7	181.7	37.5	22.4	7.3	6.2
400	201.4	211.4	55.6	18.8	6.7	5.0
500	698.3	481.7	191.0	148.8	6.6	5.1

3.2.3 Effect of electrolyte temperature

The effect of electrolyte temperature on indium cyclone electrowinning was investigated under the following conditions: current density 80 A/m^2, electrolyte flow rate 300 L/h, and electrolysis time 20 h. As shown in Fig. 8(a), the CE increased from 76.79% to 80.15% as the temperature increased from 20 to 30 °C and then decreased gradually. When the electrolyte temperature increased to 60 °C, the CE decreased sharply to 40.24%. The recovery of indium followed a similar trend as that of CE. During the electrowinning process, indium deposition and hydrogen evolution competed at the cathode, and the kinetic process of mass transfer was enhanced by increasing temperature, causing hydrogen evolution to be an even more favorable thermodynamic reaction [39]. In addition, the indium deposits were more easily dissolved by the acid electrolyte at high temperatures, leading to a decreased CE at 50 and 60 °C. Figure 8(b) presents the effect of the electrolyte temperature on the ACV and SEC. These results indicated that the electrolyte temperature had a significant influence on the ACV and SEC. The ACV decreased linearly from 2.58 to 1.91 V with increasing electrolyte temperature from 20 to 60 °C, which was attributed to the enhanced ion diffusion and the decreased concentration overpotential at high temperature [40]. Meanwhile, the plots demonstrated that the SEC decreased from

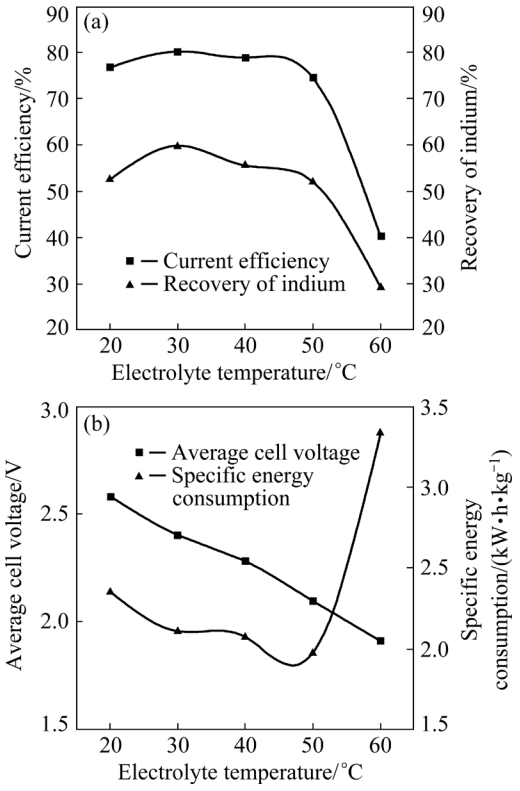

Fig. 8 Effect of electrolyte temperature on various indexes of 1st-stage indium cyclone electrowinning: (a) CE and recovery of indium; (b) ACV and SEC

2.36 to 1.98 kW·h/kg with an increase in the temperature from 20 to 50 °C, but the SEC increased sharply to 3.33 kW·h/kg because of the decreased CE.

The main impurity content in indium products at different electrolyte temperatures is shown in Table 6. When the electrolyte temperature increased from 20 to 30 °C, the content of Sn and Cd in the product decreased. However, as the temperature increased further, the contents of Sn and Cd in the product increased gradually. The electrolyte temperature had little effect on the Pb, Bi, Ni, and Fe contents in the product and maintains a low level. The effects of electrolyte temperature on the current efficiency, recovery rate, cell voltage, energy consumption and impurity content were analyzed comprehensively. A temperature of 30 °C was selected as the optimum electrolyte temperature for subsequent experiments.

Table 6 Main impurity content of cathode indium at different temperatures (10^{-6})

Electrolyte temperature/°C	Sn	Cd	Pb	Bi	Ni	Fe
20	192.2	307.8	46.0	39.5	6.3	6.3
30	136.7	181.7	37.5	22.4	7.3	6.2
40	275.4	274.1	64.4	22.3	6.1	5.8
50	326.6	293.9	84.7	20.0	7.1	5.8
60	531.3	342.6	48.8	22.7	6.9	5.9

3.2.4 Effect of electrolysis time

To investigate the effect of the electrolysis time on indium cyclone electrowinning, the experiments were conducted under the following conditions: the current density 80 A/m^2, the electrolyte flow rate 300 L/h and the electrolyte temperature 30 °C for 16, 18, 20, 22 or 24 h, respectively. As illustrated in Fig. 9, the CE decreased slightly with an increase in electrolysis time. The explanation is that with increasing electrolysis time, the concentration of indium in the electrolyte decreased, which decreased the rate of indium deposition. As the electrolysis time increased, more indium was deposited on the cathode, increasing the recovery of indium. Meanwhile, the results showed that with increasing electrolysis time, the ACV decreased slightly, as did the SEC.

Table 7 lists the main impurity content of cathode indium at different electrolysis time. It can be seen that the electrolysis time has a significant effect on the content of Sn and Cd. With increasing electrolysis time, the contents of Sn and Cd increased. Especially when the electrolysis time exceeds 22 h, the content of Sn and Cd increases sharply, which seriously reduces the purity of the product. However, the electrolysis time has little effect on the contents of impurities Pb, Bi, Ni and Fe. In summary, 20 h was selected as the optimum electrolysis time for subsequent experiments.

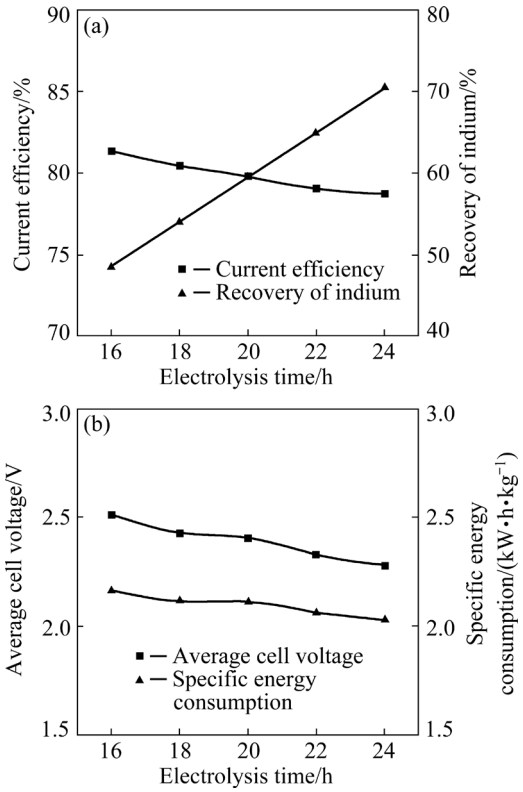

Fig. 9 Effect of electrolysis time on various indexes of 1st-stage indium cyclone electrowinning: (a) CE and recovery of indium; (b) ACV and SEC

Table 7 Main impurity content of cathode indium at different electrolysis time (10^{-6})

Electrolysis time/h	Sn	Cd	Pb	Bi	Ni	Fe
16	112.9	175.7	36.2	21.4	6.1	5.8
18	125.6	178.3	36.4	21.7	6.3	5.9
20	136.7	181.7	37.5	22.4	7.3	6.2
22	243.6	283.9	37.7	22.2	7.2	6.2
24	336.4	386.8	37.2	22.6	6.8	6.5

3.2.5 Characterization of indium deposits

Based on the results above, the optimum

conditions of 1st-stage indium cyclone electrowinning were found to be current density of 80 A/m^2, electrolyte flow rate of 300 L/h, electrolyte temperature of 30 °C, and electrolysis time of 20 h. Under these conditions, 80.15% CE, 2.11 kW·h/kg SEC, 66.39% indium recovery, and 2.04 V of ACV were achieved. Table 8 lists the chemical composition of the indium deposits obtained under the optimum conditions. The purity of indium reached 99.95%. Compared with crude indium, the purity of indium is significantly improved. Figure 10 presents the XRD pattern of the indium deposits. The diffraction peaks were in good agreement with the standard card profile of elemental indium (PDF# 85-1409). The preferred crystallographic orientations of indium deposits were in the order of (101), (110), (112) and (211).

Table 8 Chemical composition of indium deposits obtained in 1st-stage cyclone electrowinning

Purity/%	Impurities content/10^{-6}					
	Sn	Cd	Pb	Bi	Ni	Fe
99.95	136.7	181.7	37.5	22.4	7.3	6.2

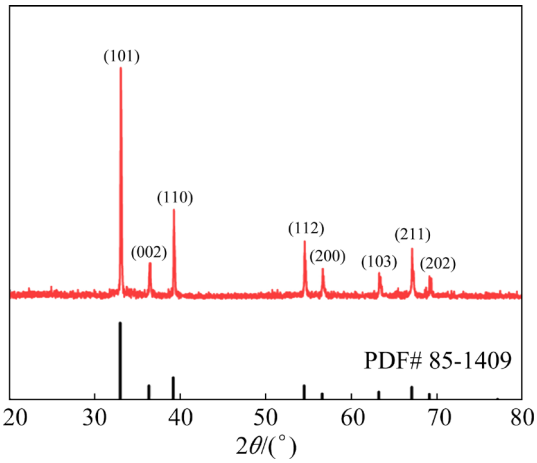

Fig. 10 X-ray diffraction pattern of indium deposits under optimum conditions

3.3 2nd-stage indium cyclone electrowinning

The spent indium electrolyte was collected after the 1st-stage electrowinning process. Table 9 lists the chemical composition of the spent indium electrolyte. This result indicated that the concentration of indium in the spent indium electrolyte was 22.92 g/L. To recover the indium in the spent electrolyte, the 2nd-stage indium cyclone electrowinning process was applied as a downstream treatment.

Table 9 Chemical composition of spent indium electrolyte (g/L)

In	Na	Bi	Pb	Sn
22.92	25.83	1.12	0.85	0.52
Si	Cd	Cu	Ni	Fe
0.43	0.35	0.04	0.02	0.01

The effects of current density, electrolysis time, electrolyte flow rate and electrolyte temperature on CE are presented in Fig. 11(a). It is observed that the CE decreased from 82.20% to 51.12% by increasing the current density from 20 to 100 A/m^2. The CE decreased slightly with increasing the electrolysis time. Increasing the flow rate from 100 to 300 L/h, the CE increased from 60.01% to 75.23%, showing that the transport-enhanced process affected the CE significantly. However, a further increase in the flow rate decreased the CE, which is due to the short circuits in the electrolytic cell. It can be seen that the CE decreased from 75.23% to 60.35% with an increase in electrolyte temperature from 30 to 60 °C. Figure 11(b) presents the effects of the current density, electrolysis time, electrolyte flow rate, and electrolyte temperature on the recovery of indium. The recovery of indium increased from 28.96% to 90.18% by increasing the current density from 20 to 100 A/m^2. The electrolysis time experiments were carried out at a current density of 60 A/m^2, and the recovery of indium increased from 68.48% to 93.56% with increasing electrolysis time from 18 to 24 h. The flow rate of the electrolyte was beneficial to the recovery of indium in the range from 100 to 300 L/h. A high electrolyte temperature harmed the deposition of indium, and the recovery of indium decreased significantly with increasing temperature. Figure 11(c) presents the effects of the current density, electrolysis time, electrolyte flow rate, and electrolyte temperature on the ACV of the electrowinning process. It is shown that increasing the current density had a significant effect on the ACV which increased from 2.12 to 2.65 V. In contrast, increasing electrolysis time and flow rate had a slight effect on ACV. Additionally, the increased temperature enhanced ion diffusion and decreased the concentration overpotential, leading to decreased cell voltage. The ACV decreased from 2.40 to 1.89 V with increasing the electrolyte temperature from 30 to 60 °C. The effects of current

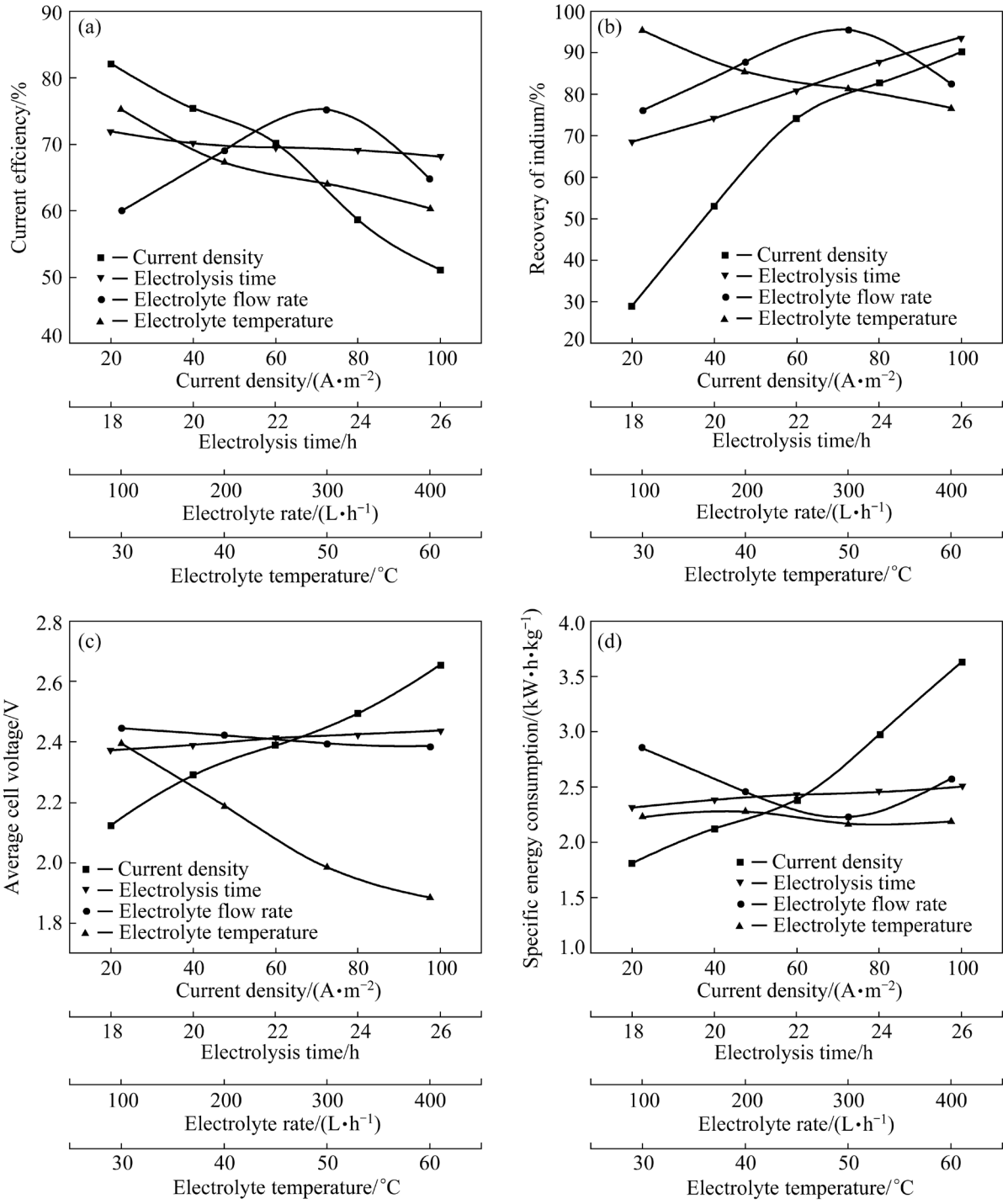

Fig. 11 Effect of different parameters on various indexes of 2nd-stage indium cyclone electrowinning: (a) CE; (b) Recovery of indium; (c) ACV; (d) SEC

density, electrolysis time, electrolyte flow rate, and electrolyte temperature on SEC are presented in Fig. 11(d). As shown in Fig. 11(d), SEC showed a sharp increase from 1.81 to 3.63 kW·h/kg with increasing the current density from 20 to 100 A/m^2. SEC increased from 2.31 to 2.50 kW·h/kg with an increase in electrolysis time. SEC decreased with increasing flow rate from 100 to 300 L/h and then increased at 400 L/h. In addition, as illustrated in Fig. 11(d), the electrolyte temperature had no significant effect on the SEC.

During the 2nd-stage electrowinning, the optimum conditions were found to be current density of 60 A/m^2, electrolysis time of 24 h, electrolyte flow rate of 300 L/h, and electrolyte temperature of 30 °C. Under these conditions,

75.23% CE, 2.23 kW·h/kg SEC, and 2.40 V of ACV were achieved. The indium recovery of the 2nd-stage cyclone electrowinning was 94.72%, and the total indium recovery of the whole process was 98.22%. Table 10 lists the chemical composition of the indium deposits obtained in the 2nd-stage cyclone electrowinning. Table 10 shows that the contents of impurities Sn, Cd, Pb and Bi in the product are relatively high. This is because impurities are easier to codeposit with the host metal when the host metal concentration is lower. The purity of the indium deposits was 98.95%. As presented in Table 11, the indium concentration in the electrolyte after the 2nd-stage cyclone electrowinning was 1.21 g/L, which can be recovered by solvent extraction. The impurities in the solution can be purified by adjusting to weak acidity followed by sodium sulfide precipitation.

Based on the mechanism described above and the optimized experimental results, a two-stage cyclone electrowinning process is proposed.

Table 10 Chemical composition of 2nd-stage indium deposits (wt.%)

In	Sn	Cd	Pb	Bi	Ni	Fe
98.95	0.41	0.28	0.21	0.12	4.02×10^{-5}	1.15×10^{-5}

Table 11 Chemical composition of electrolyte after 2nd-stage cyclone electrowinning (g/L)

In	Na	Bi	Pb	Sn
1.21	40.33	0.83	0.65	0.36
Cd	Si	Cu	Ni	Fe
0.24	0.37	0.04	0.01	0.01

Table 12 shows the process parameters and key performance indicators of the proposed process and Fig. 12 shows the flowsheet. The obtained products can be directly applied to fields with low requirements for purity of indium or further purified by vacuum distillation. In industry, crude indium sulfate solution can be directly electrochemically recovered and purified by two-stage cyclone electrowinning without sulfuric acid dissolution.

Table 12 Process parameters and key performance indicators of proposed process

Process parameter or key performance indicator	1st-stage electrowinning	2nd-stage electrowinning
Crude indium purity/%	94.34	94.34
Product purity/%	99.95	98.95
Initial concentration/(g·L^{-1})	68.20	22.92
Final concentration/(g·L^{-1})	22.92	1.21
Recovery/%	98.22	98.22
Current density/(A·m^{-2})	80	60
Electrolyte flow rate/(L·h^{-1})	300	300
Electrolyte temperature/°C	30	30
Electrolysis time/h	20	24
CE/%	80.15	75.23
SEC/(kW·h·kg^{-1})	2.11	2.23
ACV/V	2.04	2.40

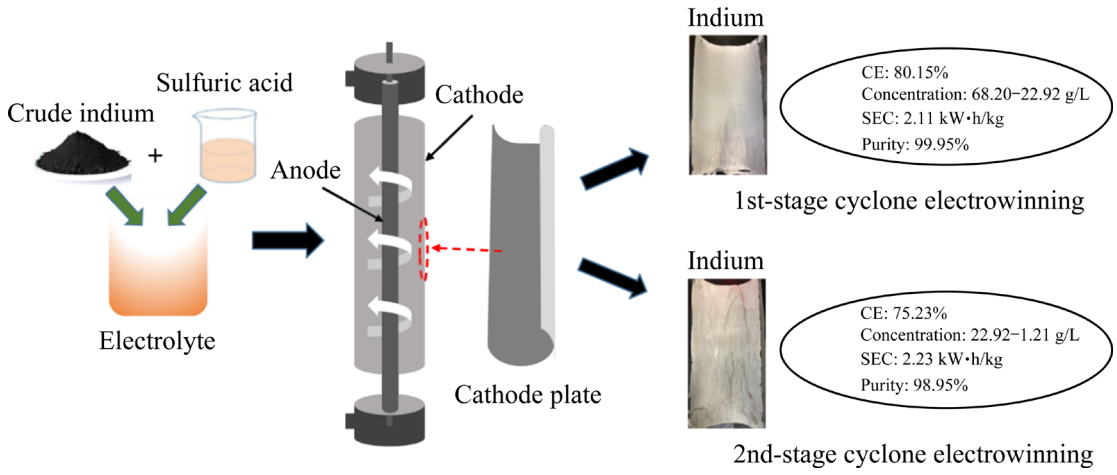

Fig. 12 Proposed flowsheet for efficient electrochemical recovery of indium by two-stage cyclone electrowinning

4 Conclusions

(1) In accordance with a linear sweep voltammetry (LSV) study and the evaluation of the diffusion coefficient (D=6.15×10^{-11} cm^2·s^{-1}), indium electrodeposition in $In_2(SO_4)_3$ solution is controlled by a diffusion-controlled irreversible process, and mass transfer can be significantly enhanced by electrolyte flow.

(2) During the 1st-stage indium cyclone electrowinning, a CE of 80.15%, SEC of 2.11 kW·h/kg, and ACV of 2.04 V were achieved under the optimum conditions: current density of 80 A/m^2, electrolyte flow rate of 300 L/h, electrolyte temperature of 30 °C and electrolysis time of 20 h. Meanwhile, the purity of indium increased from 94.34% to 99.95%. The indium concentration in the electrolyte was reduced from 68.20 to 22.92 g/L.

(3) During the 2nd-stage indium cyclone electrowinning, 98.95% of cathode indium was conducted electrowinning at 30 °C for 24 h with current density of 60 A/m^2 and electrolyte flow rate of 300 L/h, while the CE and SEC were 75.23% and 2.23 kW·h/kg, respectively. After two-stage cyclone electrowinning, the indium concentration in the electrolyte was reduced to less than 1.21 g/L, with a total indium recovery of 98.22%.

Acknowledgments

This study was financially supported by the National Natural Science Foundation of China (Nos. 52074363, 52104355, 51922108, U20A20273) and the National Key Research and Development Program of China (Nos. 2019YFC1907402, 2018YFC1902501).

References

[1] XU L, XIONG Y H, MENG J W, WANG J B, HUA Z S, TIAN Y P, YOU J L, ZHAO Z. Redox behavior of indium in molten chlorides [J]. Transactions of Nonferrous Metals Society of China, 2021, 31(5): 1496−1505.

[2] NAYAK S, DEVI N. Development of hydrometallurgical process for indium recovery from waste liquid crystal display using Cyphos IL 101 [J]. Transactions of Nonferrous Metals Society of China, 2020, 30(9): 2556−2567.

[3] MATSUMIYA M, SUMI M, UCHINO Y, YANAGI I. Recovery of indium based on the combined methods of ionic liquid extraction and electrodeposition [J]. Separation and Purification Technology, 2018, 201: 25−29.

[4] ZHOU Z H, MO H B, ZENG D M. Preparation of high-purity indium by electrorefining [J]. Transactions of Nonferrous Metals Society of China, 2004, 14(3): 637−640.

[5] KANG H N, LEE J Y, KIM J Y. Recovery of indium from etching waste by solvent extraction and electrolytic refining [J]. Hydrometallurgy, 2011, 110(1/2/3/4): 120−127.

[6] LEE M S, OH Y J. Analysis of ionic equilibria and electrowinning of indium from chloride solutions [J]. Scandinavian Journal of Metallurgy, 2004, 33(5): 279−285.

[7] ZHONG X C, ZHANG B, LIN Z C, LIU J M, XIE Y M, XU Z F. Preparation and performance of 3D-Pb anodes for nonferrous metals electrowinning in H_2SO_4 aqueous solution [J]. Transactions of Nonferrous Metals Society of China, 2020, 30(2): 535−547.

[8] ZHANG W, ROBICHAUD M, GHALI E, HOULACHI G. Electrochemical behavior of mesh and plate oxide coated anodes during zinc electrowinning [J]. Transactions of Nonferrous Metals Society of China, 2016, 26(2): 589−598.

[9] LU J, YANG Q H, ZHANG Z. Effects of additives on nickel electrowinning from sulfate system [J]. Transactions of Nonferrous Metals Society of China, 2010, 20(Suppl.): 97−101.

[10] SU J L, LIN X, ZHENG S L, NING R, LOU W B, JIN W. Mass transport-enhanced electrodeposition for the efficient recovery of copper and selenium from sulfuric acid solution [J]. Separation and Purification Technology, 2017, 182: 160−165.

[11] WANG Y T, XUE Y D, SU J L, ZHENG S, LEI H, CAI W Q, JIN W. Efficient electrochemical recovery of dilute selenium by cyclone electrowinning [J]. Hydrometallurgy, 2018, 179: 232−237.

[12] XU Z P, LI Z J, LI D, GUO X Y, YANG Y, TIAN Q H, LI J. Selective recovery of tellurium from the tellurium-bearing sodium carbonate slag by sodium sulfide leaching followed by cyclone electrowinning [J]. Metals, 2020, 10(9): 1176.

[13] JIN W, SU J L, CHEN S F, LI P, MOATS M S, MADURAIVEERAN G, LEI H. Efficient electrochemical recovery of fine tellurium powder from hydrochloric acid media via mass transfer enhancement [J]. Separation and Purification Technology, 2018, 203: 117−123.

[14] LI B, WANG X B, WEI Y G, WANG H, BARATI M. Extraction of copper from copper and cadmium residues of zinc hydrometallurgy by oxidation acid leaching and cyclone electrowinning [J]. Minerals Engineering, 2018, 128: 247−253.

[15] TIAN Q H, LI J, GUO X Y, LI D, YANG Y, XU Z P, LI W. Efficient electrochemical recovery of tellurium from spent electrolytes by cyclone electrowinning [J]. Journal of Sustainable Metallurgy, 2021, 7(1): 27−45.

[16] GUO X Y, QIN H, TIAN Q H, LI D. Recovery of metals from waste printed circuit boards by selective leaching combined with cyclone electrowinning process [J]. Journal of Hazardous Materials, 2020, 384: 121355.

[17] XU Z P, GUO X Y, TIAN Q H, LI D, ZHANG Z, ZHU L. Electrodeposition of tellurium from alkaline solution by cyclone electrowinning [J]. Hydrometallurgy, 2020, 193: 105316.

[18] WANG Y, LI B, WEI Y G, WANG H. Effect of Zn^{2+} on the extraction of copper by cyclone electrowinning from simulated copper-containing electrolyte [J]. Separation and Purification Technology, 2022, 282: 120014.

[19] WATANABE C, NOBE K. Electrochemical behaviour of indium in H_2SO_4 [J]. Journal of Applied Electrochemistry, 1976, 6(2): 159−162.

[20] HAKOMORI S I. The electrode potential of indium against indium chloride solutions [J]. Journal of the American Chemical Society, 1930, 52(6): 2372−2376.
[21] CHUNG Y, LEE C W. Electrochemical behaviors of indium [J]. Journal of Electrochemical Science and Technology, 2012, 3(1): 1−13.
[22] HATTOX E M, VRIES T D. The thermodynamics of aqueous indium sulfate solutions [J]. Journal of the American Chemical Society, 1936, 58(11): 2126−2129.
[23] KANGRO W, WEINGÄRTNER F. The electrochemistry of indium [J]. Journal of Electrochemistry, Reports of Bunsengesellschaft for Physical Chemistry, 1954, 58(7): 505−515. (in German)
[24] LIETZKE M, STOUGHTON R. The thermodynamics of indium sulfate solutions [J]. Journal of the American Chemical Society, 1956, 78(18): 4520−4526.
[25] COVINGTON A, HAKEEM M, WYNNE-JONES W. Standard potential of the In/In^{3+} electrode [J]. Journal of the Chemical Society (Resumed), 1963, 842: 4394−4401.
[26] HAMPSON N, PIERCY R. The potential of the In^{3+}/In electrode [J]. Journal of Electroanalytical Chemistry and Interfacial Electrochemistry, 1974, 51(1): 91−97.
[27] WALSH F C, GABE D R. The electrodeposition of indium [J]. Surface Technology, 1981, 13(2): 305−314.
[28] SHI M Q, MIN X B, SHEN C, CHAI L Y, KE Y, YAN X, LIANG Y J. Separation and recovery of copper in Cu−As-bearing copper electrorefining black slime by oxidation acid leaching and sulfide precipitation [J]. Transactions of Nonferrous Metals Society of China, 2021, 31(4): 1103−1112.
[29] ZHU Z L, LIU H, CHEN J S Y, KONG H, XU L, HUA Z S, ZHAO Z. Electrochemical behavior and electrolytic preparation of lead in eutectic NaCl−KCl melts [J]. Transactions of Nonferrous Metals Society of China, 2020, 30(9): 2568−2576.
[30] LIU A M, GUO M X, LÜ Z Y, ZHANG B G, LIU F G, TAO W J, YANG Y J, HU X W, WANG Z W, LIU Y B. Electrochemical behavior of tantalum in ethylene carbonate and aluminum chloride solvate ionic liquid [J]. Transactions of Nonferrous Metals Society of China, 2020, 30(8): 2283−2292.
[31] WANG X M, ZHANG F Q. Influence of anions in phosphate and tetraborate electrolytes on growth kinetics of microarc oxidation coatings on Ti6Al4V alloy [J]. Transactions of Nonferrous Metals Society of China, 2022, 32(7): 2243−2252.
[32] KHEZRI M, REZAI B, ABDOLLAHZADEH A A, WILSON B P, MOLAEINASAB M, LUNDSTRÖM M. Cyclic voltammetry and potentiodynamic polarization studies of chalcopyrite concentrate in glycine medium [J]. Transactions of Nonferrous Metals Society of China, 2021, 31(2): 545−554.
[33] DEFERM C, MALAQUIAS J C, ONGHENA B, BANERJEE D, LUYTEN J, OOSTERHOF H, FRANSAER J, BINNEMANS K. Electrodeposition of indium from the ionic liquid trihexyl(tetradecyl)phosphonium chloride [J]. Green Chemistry, 2019, 21(6): 1517−1530.
[34] ESTAGER J, NOCKEMANN P, SEDDON K R, SRINIVASAN G, SWADZBA-KWASNY M. Electrochemical synthesis of indium(0) nanoparticles in haloindate(III) ionic liquids [J]. Chemsuschem, 2012, 5(1): 117−124.
[35] AWE S A, SUNDKVIST J E, BOLIN N J, SANDSTROM A. Process flowsheet development for recovering antimony from Sb-bearing copper concentrates [J]. Minerals Engineering, 2013, 49: 45−53.
[36] NICOL M, AKILAN C, TJANDRAWAN V, GONZALEZ J A. Effect of halides in the electrowinning of zinc. II: Corrosion of lead−silver anodes [J]. Hydrometallurgy, 2017, 173: 178−191.
[37] DELL'ERA A, ZULETA E C, PASQUALI M, LUPI C. Process parameters affecting the efficiency of indium electrowinning results from sulfate baths [J]. Hydrometallurgy, 2020, 193: 105296.
[38] RIGBY G D, GRAZIER P E, STUART A D, SMITHSON E P. Gas bubble induced mixing in electrowinning baths [J]. Chemical Engineering Science, 2001, 56(21/22): 6329−6336.
[39] SAFIZADEH F, SU C, GHALI E, HOULACHI G. The effect of lead and some operating parameters on cathode contamination during zinc electrowinning [J]. Hydrometallurgy, 2017, 171: 69−76.
[40] AWE S A, SANDSTROM A. Electrowinning of antimony from model sulphide alkaline solutions [J]. Hydrometallurgy, 2013, 137: 60−67.

两段旋流电积法提纯粗铟

田庆华[1,2]，董 波[1]，郭学益[1,2]，李 栋[1,2]，黎邹江[1]，许志鹏[1,2]

1. 中南大学 冶金与环境学院，长沙 410083；
2. 中南大学 有色金属资源循环利用国家地方联合工程研究中心，长沙 410083

摘 要：采用两段旋流电积工艺对粗铟进行提纯。根据线性扫描伏安法(LSV)研究结果及对扩散系数(D=6.15×10^{-11} $cm^2\cdot s^{-1}$)的评估可知，硫酸铟溶液中铟电沉积是受扩散控制的不可逆过程，可通过加强电解质流动强化液相传质。在第一段旋流电积提纯粗铟的最佳工艺条件下，电流效率达 80.15%，单位能耗为 2.11 kW·h/kg，平均槽电压为 2.04 V，粗铟纯度由 94.34%提升至 99.95%。在第二段旋流电积提纯粗铟的最佳工艺条件下，电流效率为 75.23%，单位能耗为 2.23 kW·h/kg，平均槽电压为 2.40 V，产品纯度为 98.95%。经过二段旋流电积后，铟综合回收率高达 98.22%。

关键词：铟；旋流电积；电化学行为；提纯

(Edited by Bing YANG)